ACS Photonics

pubs.acs.org/journal/apchd5

Article

Ultrahigh Deep-Ultraviolet Responsivity of a β-Ga_2O_3/MgO Heterostructure-Based Phototransistor

Jungho Ahn, Jiyeon Ma, Doeon Lee, Qiubao Lin, Youngseo Park, Oukjae Lee, Sangwan Sim, Kyusang Lee,* Geonwook Yoo,* and Junseok Heo*

Cite This: *ACS Photonics* 2021, 8, 557−566

Read Online

ACCESS | Metrics & More | Article Recommendations | Supporting Information

ABSTRACT: Deep-ultraviolet (DUV) photodetectors based on wide-band-gap semiconductors have attracted significant interest across a wide range of applications in the industrial, biological, environmental, and military fields due to their solar-blind nature. As one of the most promising wide-band-gap materials, β-Ga_2O_3 provides great application potential over detection wavelengths ranging from 230 to 280 nm owing to its superior optoelectronic performance, stability, and compatibility with conventional fabrication techniques. Although various innovative approaches and device configurations have been applied to achieve highly performing β-Ga_2O_3 DUV photodetectors, the highest demonstrated responsivity of the β-Ga_2O_3 photodetectors has only been around 10^5 A/W. Here, we demonstrate a β-Ga_2O_3 phototransistor with an ultrahigh responsivity of 2.4×10^7 A/W and a specific detectivity of 1.7×10^{15} Jones, achieved by engineering a photogating effect. A β-Ga_2O_3/MgO heterostructure with an Al_2O_3 encapsulation layer is employed not only to reduce photogenerated electron/hole recombination but also to suppress the photoconducting effects at the back-channel surface of the β-Ga_2O_3 phototransistor via a defect-assisted charge transfer mechanism. The measured photoresponsivity is almost 2 orders of magnitude higher than the highest previously reported value in a β-Ga_2O_3-based photodetector, to the best of our knowledge. We believe that the demonstrated β-Ga_2O_3/MgO heterostructure configuration, combined with its facile fabrication method, will pave the way for the development of ultrasensitive DUV photodetectors utilizing oxide-based wide-band-gap materials.

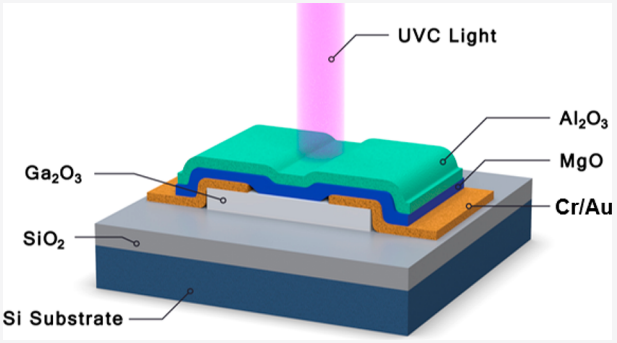

KEYWORDS: *β-Ga_2O_3, photogating effect, phototransistor, charge transfer, deep ultraviolet, ultrahigh responsivity*

The optoelectronic properties of ultra-wide-band-gap materials such as AlGaN,[1] $Mg_xZn_{1-x}O$,[2] $Zn_xGa_{1-x}O$,[3,4] BN,[5] and diamond[6,7] have enabled the implementation of solar-blind deep ultraviolet (DUV) photodetectors for unique applications such as flame detection,[1,8,9] missile tracking,[7] pollution monitoring, and intersatellite communication systems. The high thermal stability, high chemical stability, and superior radiation hardness of these materials also enable them to be deployed in harsh conditions, such as high-temperature environments and space. Despite substantial progress in crystal growth technologies over the past few decades, obtaining high-quality ultra-wide-band-gap alloys is still challenging because of their demanding growth conditions and poor crystalline quality.[10−12] For instance, a lattice-mismatched heteroepitaxial growth of AlGaN, and a phase mixing in a high-Mg-content MgZnO, resulted in a large defect density, degrading detecting performance.[11−14] As alternatives to these materials for DUV photodetection, monoclinic β-Ga_2O_3, the most stable phase in the polymorphism of Ga_2O_3, holds promise. Its well-developed melt growth methods, such as the Czochralski method, edge-defined film-fed growth, and the floating zone technique, allow the production of single-crystal β-Ga_2O_3 wafers with superior material quality.[15−18] In addition, β-Ga_2O_3 active layers obtained by mechanical exfoliation[19−21] or homoepitaxy[22] from single-crystal bulk substrates have demonstrated high crystal quality, making them promising contenders for solar-blind high-performance DUV photodetectors.

The figure of merit for DUV photodetectors in particular is responsivity (in A/W), which is inversely proportional to the energy of a detected photon and proportional to the quantum efficiency.[23] The responsivity can be improved by maximizing the absorption of incident light and/or by extracting more carriers per photon. The former strategy was pursued by employing UV-transparent electrodes such as semitransparent Ni/Au,[24] IZO,[25] and graphene;[19,26,27] nevertheless, this

Received: October 11, 2020
Published: January 12, 2021

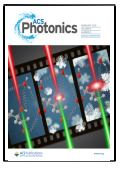

https://dx.doi.org/10.1021/acsphotonics.0c01579
ACS Photonics 2021, 8, 557−566

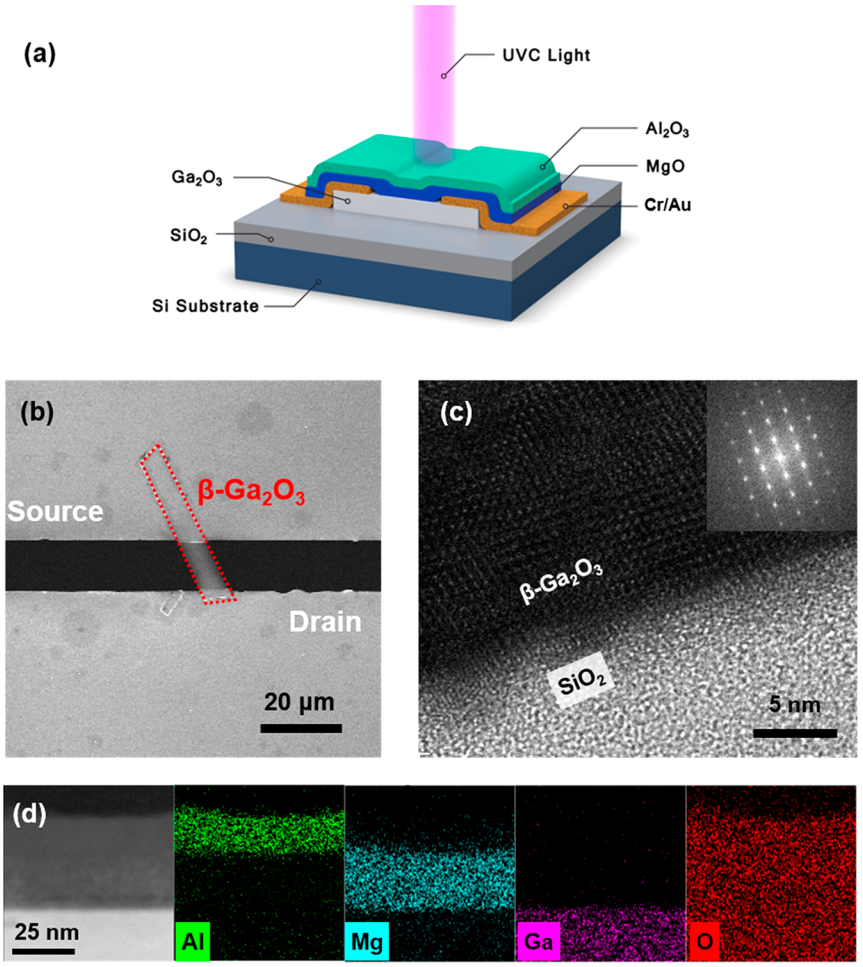

Figure 1. (a) Schematic illustration of the β-Ga_2O_3/MgO heterostructure-based phototransistor. (b) Scanning electron microscope (SEM) image of the fabricated β-Ga_2O_3/MgO phototransistor. Scale bar: 20 μm. (c) High-resolution TEM image of the β-Ga_2O_3/SiO_2 interface. Scale bar: 5 nm. Inset: corresponding FFT patterns of the β-Ga_2O_3 region. (d) EDX elemental mapping of four chemical species (Al, Mg, Ga, and O). Scale bar: 25 nm.

approach by itself cannot overcome the maximum imposed by the intrinsic material responsivity. The latter strategy achieves higher responsivity by means of avalanche carrier multiplication or unbalanced channel-charge-induced photocurrent gain.[28] In this context, various types of β-Ga_2O_3 photodetector configurations with a photocurrent gain mechanism have been investigated, including metal−semiconductor−metal devices, heterojunctions, and phototransistors. Still, the highest responsivity achieved for the β-Ga_2O_3 photodetector has been ~10^5 A/W.[21]

In this work, we demonstrate a β-Ga_2O_3/MgO heterostructure DUV phototransistor with ultrahigh sensitivity by using the photogating effect to significantly amplify the photocurrent. MgO and Al_2O_3 layers are sputtered by a radio frequency (RF) magnetron on top of a β-Ga_2O_3 phototransistor on a Si/SiO_2 substrate, where the heavily doped Si substrate is used to control a gate. The material properties of the β-Ga_2O_3/MgO/Al_2O_3 layers were characterized by high-resolution transmission electron microscopy (HR-TEM) and energy-dispersive X-ray spectroscopy (EDX). Furthermore, the optoelectronic properties of the β-Ga_2O_3 and β-Ga_2O_3/MgO phototransistors were characterized under illumination with DUV light and dark conditions. A comparison between the β-Ga_2O_3 and β-Ga_2O_3/MgO heterostructure phototransistors shows that the MgO layer efficiently limits the photoconductive effect, such that the photogating effect predominantly governs the β-Ga_2O_3/MgO heterostructure-based phototransistor operation. We ascribe this phenomenon to defect-assisted charge transfer at the β-Ga_2O_3/MgO interface, where the charge transfer process could be described by electronic band diagrams. As the photogating effect is solely responsible for the significant photocurrents due to the restricted photoconduction, the β-Ga_2O_3/MgO phototransistor showed an ultrahigh responsivity of 2.4×10^7 A/W and a specific detectivity of 1.7×10^{15} Jones at the wavelength of 260 nm. These unprecedentedly high DUV responsivity and specific detectivity values confirm that the β-Ga_2O_3/MgO heterostructure-based phototransistor outperforms previously reported β-Ga_2O_3-based DUV photodetectors.

RESULTS AND DISCUSSION

Figure 1a shows the configuration of the β-Ga_2O_3 phototransistor, which included a charge transfer layer (MgO) and an encapsulation layer (Al_2O_3). Here, the β-Ga_2O_3 films (270 nm, see the Supporting Information) were mechanically exfoliated from a single-crystal (−201) bulk β-Ga_2O_3 substrate (Tamura Corp., Japan) and transferred onto a Si/SiO_2 substrate. The highly doped Si substrate was used to apply the gate voltage to the β-Ga_2O_3 channel through the SiO_2

https://dx.doi.org/10.1021/acsphotonics.0c01579
ACS Photonics 2021, 8, 557−566

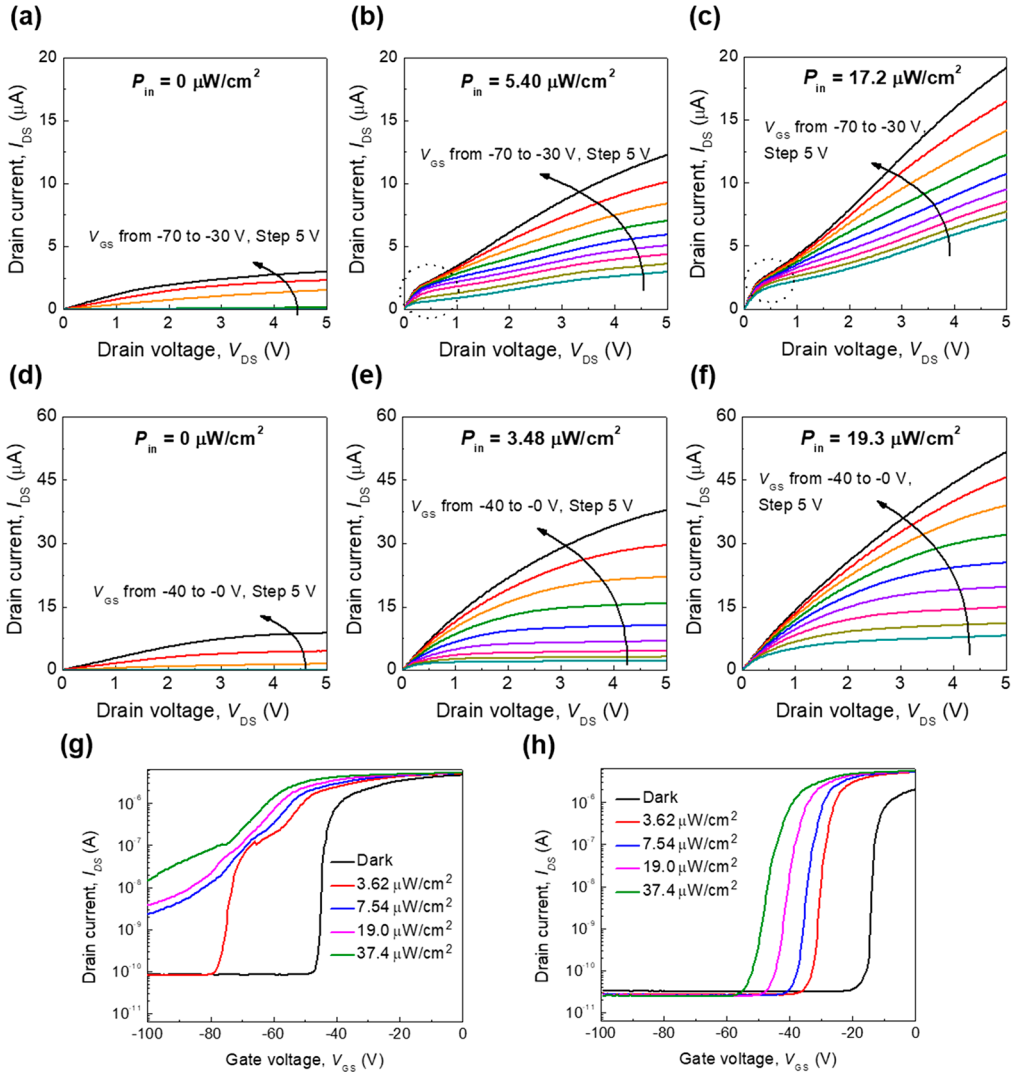

Figure 2. I_{DS}−V_{DS} characteristics of the β-Ga_2O_3 phototransistor without a MgO layer at V_{GS} values ranging from −70 to −30 V, in steps of 5 V, under (a) dark conditions and 260 nm DUV light illumination of (b) 5.40 μW/cm^2 and (c) 17.2 μW/cm.[2] I_{DS}−V_{DS} characteristics of the β-Ga_2O_3/MgO phototransistor with an Al_2O_3 encapsulation layer at V_{GS} values ranging from −40 to 0 V, in steps of 5 V, under (d) dark conditions and 260 nm DUV light illumination of (e) 3.48 μW/cm^2 and (f) 19.3 μW/cm^2. Transfer characteristics of the (g) β-Ga_2O_3 and (h) β-Ga_2O_3/MgO phototransistor. V_{DS} was fixed at 1 V.

dielectric layer. The source (S) and drain (D) electrodes (Cr/Au 20/80 nm) were deposited and patterned by thermal evaporation following a photolithography process. Then, MgO (30 nm) and Al_2O_3 (20 nm) were deposited by RF magnetron sputtering at room temperature. The Al_2O_3 encapsulation layer prevents a degradation of the MgO layer by water molecules due to a hygroscopic nature of the MgO layer.[29,30] Figure 1b shows a scanning electron microscope (SEM) image of the fabricated β-Ga_2O_3/MgO phototransistor. We also fabricated a reference β-Ga_2O_3 phototransistor with nearly identical dimensions and channel thickness to investigate the effects of the MgO layer.

Material properties of the exfoliated β-Ga_2O_3 and MgO/Al_2O_3 layers in the fabricated device were studied by using HR-TEM and an EDX mapping. Cross-sectional HR-TEM images were obtained over the SiO_2/β-Ga_2O_3/MgO/Al_2O_3 cross-sectional interface (Figure 1c; see the Supporting Information for MgO). A fast Fourier transform (FFT) micrograph of the β-Ga_2O_3 HR-TEM image indicates the high crystal quality of the exfoliated β-Ga_2O_3 film (inset of Figure 1c). Moreover, Figure 1d shows a cross-sectional TEM image and the corresponding TEM-EDX maps of the device, where four elemental species (Al, Mg, Ga, and O) are displayed as four different colors (green, cyan, magenta, and red). The TEM-EDX maps clearly reveal that the MgO and Al_2O_3 layers were uniformly deposited on top of the β-Ga_2O_3 layer.

Figure 2a−c shows the output characteristics (I_{DS}−V_{DS}) of the reference β-Ga_2O_3 device for gate biases (V_{GS}) ranging from −70 to −30 V at steps of 5 V, under dark conditions and 260 nm DUV light illumination of 5.4 or 17.2 μW/cm^2. We set the wavelength of DUV light at 260 nm, in which the photon energy is slightly larger than the band gap of β-Ga_2O_3, in this work for simplicity of the experiment (see the Supporting Information for the analysis of spectral responsivity). The I_{DS}−V_{DS} curves of the β-Ga_2O_3 device under dark conditions exhibit the typical linear and saturation characteristics of thin-film transistors (TFTs) (Figure 2a). However, the output curves of the reference device under DUV light deviate from this behavior, exhibiting a hump in the low V_{DS} region (V_{DS} < 1 V) (black dotted circles in Figure 2b,c).[31] The hump implies

https://dx.doi.org/10.1021/acsphotonics.0c01579
ACS Photonics 2021, 8, 557−566

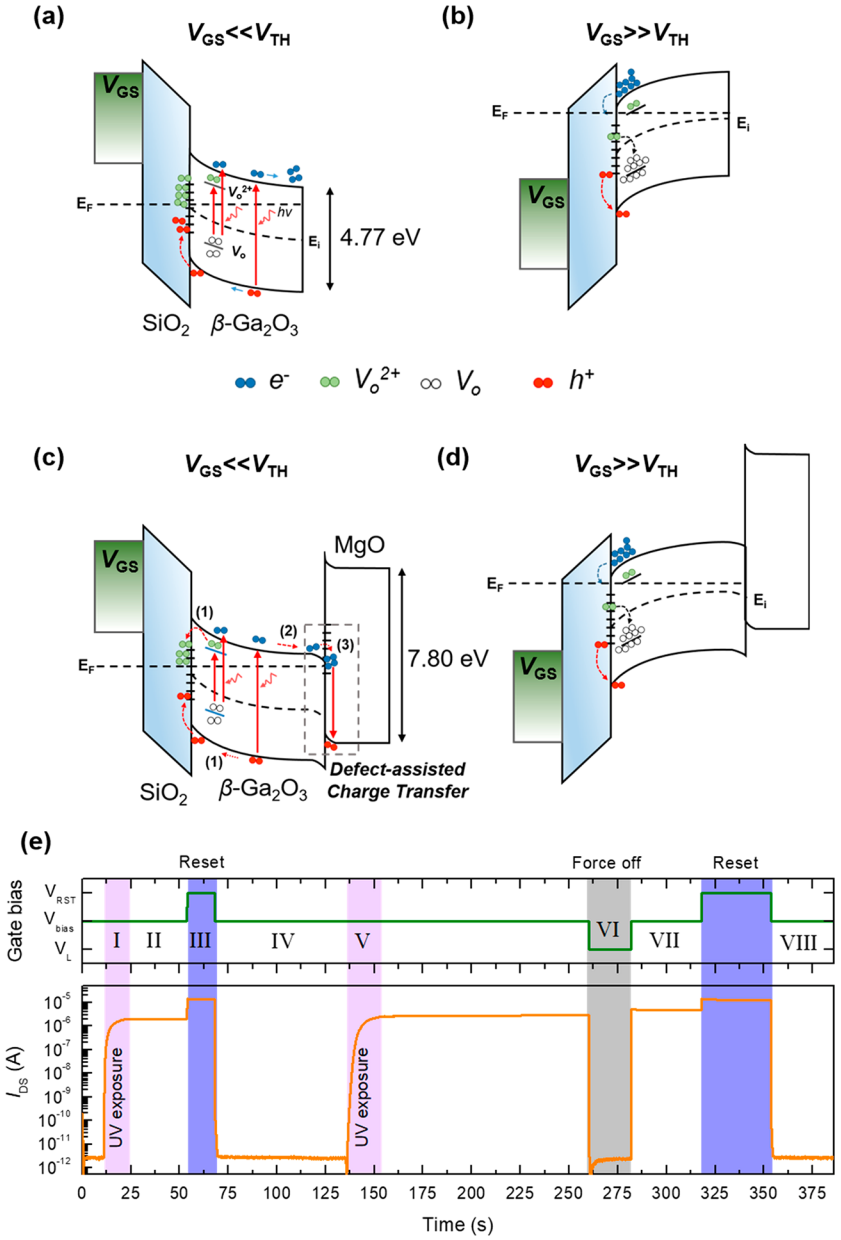

Figure 3. (a, b) Schematic illustration of the charge transport mechanisms in the β-Ga_2O_3 phototransistor without the MgO layer: (a) When the device is illuminated by DUV light under a negative gate bias, holes and ionized oxygen vacancies are trapped at the SiO_2/β-Ga_2O_3 interface while photogenerated electrons remain on the back-channel surface. (b) When a positive bias is applied to the β-Ga_2O_3 phototransistor, electrons are injected at the SiO_2/β-Ga_2O_3 interface, releasing the trapped holes and oxygen vacancies. (c, d) Schematic illustration of the charge transport mechanisms in the β-Ga_2O_3/MgO heterostructure-based phototransistor: (c) When DUV light illuminates the β-Ga_2O_3/MgO phototransistor under a negative gate bias, holes and ionized oxygen vacancies are trapped at the SiO_2/β-Ga_2O_3 interface, but the photogenerated electrons are transferred to the MgO layer by a defect-assisted charge transfer process. (d) When a positive bias is applied to the β-Ga_2O_3/MgO phototransistor, the trapped positive charges are released in the same fashion as in the β-Ga_2O_3 device. (e) Comprehensive transient response of the β-Ga_2O_3/MgO phototransistor under the application of various gate voltage pulses. The measurement is conducted under a fixed V_{DS} = 1 V, DUV irradiance = 5.4 μW/cm^2, V_{RST} = 33 V, V_{bias} = −36 V, and V_L = −69 V.

that two distinct charge transport mechanisms in the β-Ga_2O_3 channel concurrently contribute to the conduction of carriers. It has been known that the back-channel surface of metal-oxide semiconductor-based TFTs provides an additional conduction channel that is not controlled by a gate bias, thereby increasing dark current and reducing photoresponsivity.[32−36] This back-channel conduction possibly originates from photoadsorption/desorption of oxygen species from the atmosphere,[36] as the back-channel effect is only observed in the reference β-Ga_2O_3 device in which the surface is exposed to the ambient air.

To suppress the back-channel surface effects, we introduce the β-Ga_2O_3/MgO heterostructure-based phototransistor with an Al_2O_3 encapsulation layer. Figure 2d−f presents the linear and saturation output characteristics of the β-Ga_2O_3/MgO phototransistor under dark conditions, as well as under 3.48 and 19.3 μW/cm^2 light illumination. We attribute the suppression of the back-channel conduction in the β-Ga_2O_3/MgO device to defect-assisted charge transfer, which will be discussed in more detail in a later section. Figure 2g,h shows transfer characteristics of the β-Ga_2O_3 and β-Ga_2O_3/MgO

https://dx.doi.org/10.1021/acsphotonics.0c01579
ACS Photonics 2021, 8, 557−566

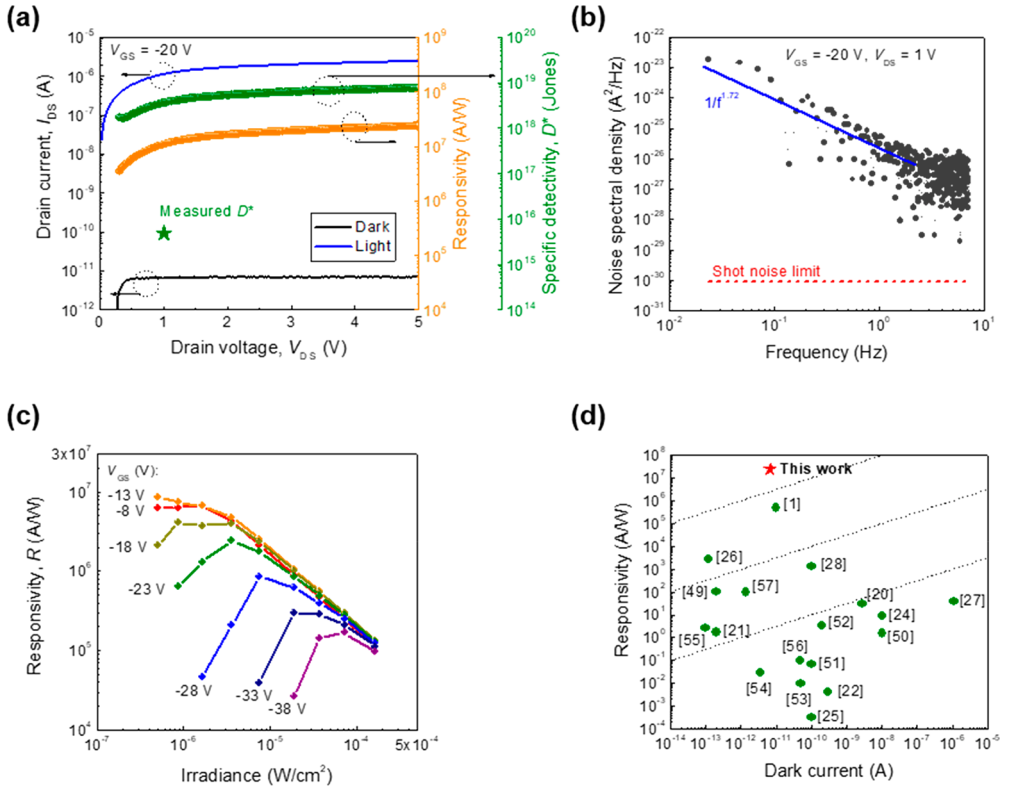

Figure 4. (a) Dependence of responsivity and specific detectivity on drain voltage (at V_{GS} = −20 V) under light illumination of 0.51 μW/cm^2. The I_{DS} curves under the dark and the light illumination are also plotted to aid understanding. (b) Noise spectral density of dark current at V_{GS} = −20 V and V_{DS} = 1 V. (c) Responsivity as a function of incident irradiance under different applied gate voltages (V_{DS} = 1 V). (d) Responsivity and dark current of several state-of-the-art β-Ga_2O_3-based phototransistors.[19−22,24−28,49−57]

phototransistors, respectively, at V_{DS} = 1 V under DUV light illumination. The threshold voltage (V_{TH}) difference of ∼30 V between the β-Ga_2O_3 and β-Ga_2O_3/MgO devices is attributed to a slight thickness difference of β-Ga_2O_3 layers in those devices since a V_{TH} of β-Ga_2O_3 transistors sensitively depends on a thickness of the β-Ga_2O_3 layer.[37] In the β-Ga_2O_3 phototransistor, a light-induced hump appears when the gate bias is lower than V_{TH}. This hump is observed because the photoconductive and photogating effects concurrently occur in the β-Ga_2O_3 phototransistors under light illumination. Although a weak photoconductive effect is measured at highly negative gate biases (V_{GS} < −80 V) under weak light illumination (P = 3.48 μW/cm^2) due to oxygen vacancy defect trapping, the coexistence of the photoconductive and photogating effects is evidenced by the two different rising slopes that exist in the transfer curves. The observed relatively high photoconductive gain may be attributed to a hole self-trapping, lowering a potential barrier between the β-Ga_2O_3 and the S/D metal at V_{GS} < V_{TH}.[38] On the other hand, only the photogating effect contributes to photocurrent generation in the β-Ga_2O_3/MgO phototransistor, which means that no photocurrent arises from photoconduction when V_{GS} < V_{TH}. By eliminating the photoconductive effect, the recombination of photogenerated electron−hole pairs is effectively suppressed, enabling ultrahigh photoresponsivity solely by means of the photogating effect.[23,39,40]

To explain the suppression of the photoconductive effect in the β-Ga_2O_3/MgO heterostructure device, we propose a defect-assisted charge transfer model. Figure 3a,b displays a schematic illustration of processes involving photogenerated charge carriers for the β-Ga_2O_3 and the β-Ga_2O_3/MgO devices, respectively, when the applied gate bias voltage is either much lower or much higher than the threshold voltage ($V_{GS} \ll V_{TH}$ or $V_{GS} \gg V_{TH}$). The drawn band diagram is based on literature values.[41−43] When photons with above-band-gap energies illuminate the phototransistor, an absorbed photon causes the creation of a free electron−hole pair as well as the ionization of an oxygen vacancy (V_0), generating two free electrons in the conduction band ($V_0 + h\nu \rightarrow V_0^{2+} + 2e^-$).[44] In the β-Ga_2O_3 phototransistor, when V_{GS} is less than V_{TH}, photogenerated holes and ionized oxygen vacancies are attracted to the SiO_2/β-Ga_2O_3 interface, while photogenerated electrons are attracted to the back-channel surface (Figure 3a). The drifting photogenerated holes and oxygen vacancies become localized by deep interfacial trap states, inducing a negative V_{TH} shift (i.e., the photogating effect).[23,39,40] At the same time, the remaining photogenerated electrons in the conduction band flow to the drain electrode, resulting in photocurrent at the below-threshold gate voltage (i.e., the photoconducting effect),[23,39,40] while some of the electrons recombine with holes, reducing the photoresponsivity. When $V_{GS} \gg V_{TH}$, electrons are injected at the SiO_2/β-Ga_2O_3 interface, and the injected electrons deionize the ionized oxygen vacancies and combine with the trapped holes (Figure 3b). Subsequently, the shift in threshold voltage is recovered. This conceptual mechanism also explains the evolution of the β-Ga_2O_3 phototransistor operation under light illumination and varying gate bias voltage, which will be discussed in Figure 3e.

While the overall mechanism for the β-Ga_2O_3/MgO heterostructure phototransistor is similar to that of the β-Ga_2O_3 phototransistor, we assume that the defect-assisted

https://dx.doi.org/10.1021/acsphotonics.0c01579
ACS Photonics 2021, 8, 557−566

Table 1. Reported Values for Dark Current, Responsivity, and Specific Detectivity in β-Ga_2O_3-Based Photodetectors[19−22,24−28,49−57]

materials	dark current (A)	responsivity (A/W)	detectivity (Jones)	operating bias (V)	rise time (s)	fall time (s)	ref
β-Ga_2O_3 flakes	6.7×10^{-12}	2.3×10^{7}	1.7×10^{15}	V_{DS} = 5, V_{GS} = −20	6.38	>1000 w/PBP: 0.07	this work
β-Ga_2O_3 flakes	2.77×10^{-9}	29.8	1.45×10^{12}	10			19
β-Ga_2O_3 flakes	2×10^{-13}	1.68	3.73×10^{10}	30	1.76	0.53	20
β-Ga_2O_3 flakes	9.91×10^{-12}	4.79×10^{5}	6.69×10^{14}	V_d = 20, V_g = −20	0.025	0.025	21
MBE-grown β-Ga_2O_3	3×10^{-10}	4×10^{-3}		5	0.1	0.1	22
β-Ga_2O_3 substrate	1×10^{-8}	8.7		10			24
MOCVD-grown β-Ga_2O_3	1×10^{-10}	3.2×10^{-4}	2.8×10^{10}	10			25
graphene/β-Ga_2O_3 flakes	1.2×10^{-13}	2.6×10^{3}	9.7×10^{13}	8	1.0/8.3	0.6/9.7	26
graphene/β-Ga_2O_3 wafer	1.1×10^{-6}	39.3	2.24×10^{12}	20	94.83	219.19	27
ZnO-Ga_2O_3 core−shell	1×10^{-10}	1.3×10^{3}	9.91×10^{14}	6	2×10^{-5}	4.2×10^{-5}	28
Ga_2O_3 nanobelt	2×10^{-13}	$\sim 10^{2}$		30	11.9	0.3	49
MBE grown β-Ga_2O_3	1×10^{-8}	1.5		4	3.33	0.4	50
β-Ga_2O_3/SiC	1×10^{-10}	7×10^{-2}		2	1.2×10^{-3}	1.5×10^{-3}	51
2D β-Ga_2O_3 nano sheet	2×10^{-10}	3.3	4.0×10^{12}	10	0.03	0.06	52
β-Ga_2O_3/ZnO	5×10^{-11}	9.7×10^{-3}	6.29×10^{12}	−2	1×10^{-4}	9×10^{-4}	53
β-Ga_2O_3/MgO	3.5×10^{-12}	0.03		10	0.07/0.53	0.06/0.16	54
PEDOTs/β-Ga_2O_3	1×10^{-13}	2.6	2.2×10^{13}	−0.5	3.4×10^{-4}	3×10^{-3}	55
β-Ga_2O_3/MgO	4.7×10^{-11}	0.1	4.3×10^{12}	5	0.231	0.032	56
β-Ga_2O_3/MgO	1.4×10^{-12}	96.13		5	0.032	0.078	57

charge transfer takes place at the β-Ga_2O_3/MgO interface under light illumination (Figure 3c), which increases the photoresponsivity by suppressing electron−hole recombination and back-channel conduction at the off state of the phototransistor. When V_{GS} is less than V_{TH}, the photogenerated holes and ionized oxygen vacancies migrate to the SiO_2/β-Ga_2O_3 interface (process 1 in Figure 3c), and the photogenerated electrons drift toward the β-Ga_2O_3 back-channel surface (process 2 in Figure 3c), where they are trapped by interfacial oxygen defect states at the SiO_2/β-Ga_2O_3 and β-Ga_2O_3/MgO junctions, respectively. Meanwhile, the trapped electrons are recombined with holes in the MgO layer by a defect-assisted nonradiative recombination process (process 3 in Figure 3c), resulting in the transfer of the photogenerated electrons in β-Ga_2O_3 to the MgO layer (defect-assisted charge transfer).[45] Consequently, the β-Ga_2O_3/MgO device functionally mitigates photogenerated electron−hole pair recombination and back-channel conduction in the β-Ga_2O_3 channel layer at the transistor off state, enabling the observed ultrahigh responsivity and high specific detectivity (to be discussed in Figure 4). When V_{GS} is greater than V_{TH} (Figure 3d), the operation mechanism is nearly identical with the β-Ga_2O_3 device without the MgO layer.

Figure 3e shows the time-resolved photoresponse of the β-Ga_2O_3/MgO phototransistor under a drain bias of 1 V, in which DUV light of an irradiance of 5.4 $\mu W/cm^2$ is used for the light-on state during the measurement. When the light is on for 10 s under a gate bias of V_{bias} = −36 V (= V_{TH} − 17 V), I_{DS} increases as the holes and ionized oxygen vacancies are trapped at the SiO_2/β-Ga_2O_3 interface, leading to the observed negative V_{TH} shift (I). After the light is turned off, the photocurrent is stable during the extremely slow recovery time, which is the so-called persistent photocurrent (PPC) (II).[44,46] PPC is commonly observed in oxide TFTs under UV light illumination due to the slow decay time of the oxygen vacancy defect states, and it prohibits a photodetector from exhibiting a fast photocurrent response. Hence, PPC is usually very desirable to implement optoelectronic memory.[47,48] To circumvent the restriction of the slow photoresponse, a positive gate bias voltage pulse (PBP, V_{RST} = 33 V = V_{TH} + 50 V) is applied to quickly suppress the PPC (III). When the PBP is applied, electrons in the channel are injected at the SiO_2/β-Ga_2O_3 interface, recombining the trapped holes and ionized oxygen vacancies with the electrons and returning the shifted V_{TH} to the initial value (IV). On the other hand, when a negative gate bias of −69 V (= V_L = V_{TH} − 50 V) is applied to the phototransistor (VI), photogenerated holes and ionized oxygen vacancies from another 10 s DUV light illumination (V_{GS} = V_{bias}) (V) remained trapped. Although the phototransistor appears to recover to the initial state while the negative gate bias is being applied, the removal of the negative gate bias restores the device to the on state (VII) since the trapped positive charges have not been released (Figure 3a,c). In fact, the drain current slightly increases after the negative gate bias is applied because extra positive charges are injected at the SiO_2/β-Ga_2O_3 interface. After these phenomena, the application of another PBP completely recovers the shift in V_{TH} (VIII). The comprehensive transient responses detailed here support the model, which is depicted in Figure 3a,c.

Based on the above discussion, the β-Ga_2O_3/MgO phototransistor is expected to exhibit an outstanding performance with high photosensitivity. The responsivity (R) and the specific detectivity (D^*) of phototransistors are key parameters for evaluating the photosensitivity and detection capability, respectively, toward low-level light in a photodetector. For further characterization of the phototransistor, the responsivity and the specific detectivity are characterized under various V_{DS}, V_{GS}, and irradiance conditions. The responsivity is given by $R = I_{ph}/(PA)$, where P and A are the incident light power and the effective illuminated area of the device, respectively, and the specific detectivity can be expressed as $D^* = (A \cdot BW)^{1/2}/NEP$, where BW is the bandwidth, and NEP is the noise-equivalent power. When we assume that the major factor of the noise of the phototransistor is dominated by the shot noise, the specific detectivity can be expressed ad $D^* = R \cdot A^{1/2}/(2eI_{dark})^{1/2}$, where e is the electron charge. Therefore, the responsivity and the

https://dx.doi.org/10.1021/acsphotonics.0c01579
ACS Photonics 2021, 8, 557−566

specific detectivity can be calculated using the measured I_{ph} and I_{dark}. Figure 4a shows the responsivity and specific detectivity as a function of V_{DS} (at V_{GS} = −20 V) under 0.51 μW/cm^2 light illumination. The I_{DS} curves under dark conditions and light illumination are also plotted to aid understanding. Both R and D^* obviously increase with increasing V_{DS} due to the increase of I_{ph}, and they saturate at high V_{DS}, where R and D^* are 2.1 × 10^7 A/W and 1.8 × 10^{15} Jones, respectively, at V_{DS} = 5 V (Figure 4a). The shot noise limited D^* is prone to overestimate the performance because other noise components are not considered. Thus, a noise analysis of dark current is beneficial to precisely predict a specific detectivity. Figure 4b shows the noise spectral density of dark current at V_{GS} = −20 V and V_{DS} = 1 V. It turns out that the flicker noise proportional to $1/f^{1.72}$ prevails in the noise spectrum. The rms (root mean squared) value of the noise current up to BW = 1 Hz was 1.11 pA, corresponding to D^* of 4.9 × 10^{15} Jones. The measured D^* determined by the noise analysis was 3 orders of magnitude lower than the shot noise limited D^* as shown in Figure 4a. Nevertheless, the measured D^* of ∼10^{15} is still an unprecedentedly high value. Figure 4c shows the responsivity as a function of the irradiance under different applied gate voltages. Since the photogating effect is predominantly attributed to the generation of photocurrent by the shift in V_{TH}, the responsivity increases with increasing irradiance until the effective threshold voltage ($V_{TH,eff} = V_{TH} + \Delta V_{TH}$) is equal to the applied gate voltage. When $V_{TH,eff}$ is higher than the applied gate voltage, the responsivity decreases with increasing light intensity. This decrease could be caused by absorption saturation, as well as by enhanced scattering and/or recombination rates associated with high irradiance.

On the basis of the analyzed characteristics of the β-Ga_2O_3/MgO phototransistor, we obtain ultrahigh values of R = 2.4 × 10^7 A/W and D^* = 1.7 × 10^{15} Jones at V_{DS} = 5 V, V_{GS} = −20 V, and P = 0.51 μW/cm^2 in the β-Ga_2O_3/MgO device. Figure 4d shows the responsivities and dark current values for several previously reported β-Ga_2O_3 photodetectors based on exfoliated β-Ga_2O_3, MBE- or MOCVD-grown β-Ga_2O_3, and β-Ga_2O_3 heterostructures.[19−22,24−28,49−57] It should be noted that, to the best of our knowledge, the achieved responsivity in this work is almost 2 orders of magnitude higher than the best previously reported responsivity for β-Ga_2O_3-based photodetectors.[21] However, the β-Ga_2O_3/MgO phototransistor has a slow response speed compared to other reported photoconductive-type photodetectors (Table 1) since a trade-off between responsivity and bandwidth exists in photogating-type photodetectors.[23] An effective method to overcome the extremely slow recovery time (>1000 s) is an application of a PBP to release trapped positive charges at the SiO_2/β-Ga_2O_3 interface as shown in Figure 3e. With a use of the PBP, the recovery time reduces to 70 ms (Figure S3), which is comparable to that of other β-Ga_2O_3-based photodetectors. A real-time detection of an extreme weak DUV light could also be achievable by using periodic PBP.[47]

CONCLUSIONS

In summary, we have demonstrated a β-Ga_2O_3/MgO heterostructure-based DUV phototransistor with an Al_2O_3 encapsulation layer, exhibiting ultrahigh light sensitivity. The material properties were characterized by HR-TEM and TEM-EDX mapping, confirming the highly crystalline quality of the β-Ga_2O_3. We studied the β-Ga_2O_3 and β-Ga_2O_3/MgO phototransistors under 260 nm light illumination and compared the β-Ga_2O_3/MgO device to the β-Ga_2O_3 device to clarify the role of the MgO layer. The MgO layer effectively suppressed the photoconductive current in the subthreshold region and enhanced a photogating effect by defect-assisted charge transfer at the β-Ga_2O_3/MgO interface. Due to this charge transfer, the recombination of photogenerated electrons and holes is inhibited, contributing to the enhancement of the photogating effect and the photocurrent. As a result, we are able to achieve the highest responsivity (2.3 × 10^7 A/W) and specific detectivity (1.7 × 10^{15} Jones) of any reported β-Ga_2O_3 photodetection device. The β-Ga_2O_3/MgO phototransistor can be applied to applications, which require a detection of ultraweak DUV light (<1 μW/cm^2), such as flame and radiation detection and astronomical studies. Moreover, this β-Ga_2O_3/MgO heterostructure configuration will provide a promising way for the development of ultrasensitive DUV photodetectors utilizing oxide-based wide-band-gap materials.

EXPERIMENTAL SECTION

Device Fabrication. Single-crystal β-Ga_2O_3 flakes were mechanically exfoliated from a 15 mm × 10 mm (−201) surface β-Ga_2O_3 bulk substrate with an unintentional n-type doping concentration of 4.8 × 1017 cm^{-3} (Tamura Corp., Japan) using a conventional Scotch tape exfoliation method and then transferred onto a heavily doped p-type Si substrate with a thermally grown 300 nm SiO_2 layer. The surface was cleaned in acetone and IPA for 20 min prior to the transfer, and then, source and drain electrodes of Cr/Au (20/80 nm) were deposited by thermal evaporation and patterned using conventional photolithography and lift-off processes. After that, a dielectric MgO layer (30 nm), followed by Al_2O_3 (20 nm), was deposited by radio frequency (RF) magnetron sputtering at room temperature. The MgO layer was sputtered from a MgO target under Ar gas injection at 3 mTorr working pressure and 100 W RF power, in which a deposition rate was 2 Å/min. Finally, the source/drain contacts were opened via buffered oxide etchant (BOE).

Optoelectrical Device Characterization. Electrical properties and photoresponses of the devices were characterized using a source meter (2614B, Keithley) and a deep-UV light-emitting diode (LED260J, Thorlabs). The UV LED exhibited a peak wavelength centered at 260 nm and a full width at half-maximum of 12 nm. For photoresponse measurements, the illumination power densities were varied from 0.51 to 180 μW/cm^2 by adjusting the current applied to the UV LED. To avoid any artifacts induced by slow detrapping of photocarriers, the consistency of the electrical characteristics under dark conditions was confirmed between each photocurrent measurement. Comprehensive transient characteristics were measured with a drain-source voltage of 1 V and an irradiance of 5.4 μW/cm^2. After deep UV exposure at a gate bias of −36 V (V_{bias}), pulses of either 33 V (V_{RST}) or −69 V (V_L) were applied to the gate.

ASSOCIATED CONTENT

Supporting Information

The Supporting Information is available free of charge at https://pubs.acs.org/doi/10.1021/acsphotonics.0c01579.

Cross-sectional HR-TEM image and diffraction patterns; spectral responsivity analysis; response/recovery time; cross-sectional TEM image; spectral noise power

https://dx.doi.org/10.1021/acsphotonics.0c01579
ACS Photonics 2021, 8, 557−566

density; transmission spectrum; and transfer characteristics of other devices (PDF)

AUTHOR INFORMATION

Corresponding Authors

Kyusang Lee − *Department of Electrical and Computer Engineering, University of Virginia, Charlottesville, Virginia 22904, United States*; Email: kl6ut@virginia.edu

Geonwook Yoo − *School of Electronic Engineering, Soongsil University, Seoul 06938, South Korea*; orcid.org/0000-0002-7826-9005; Email: gwyoo@ssu.ac.kr

Junseok Heo − *Department of Electrical and Computer Engineering, Ajou University, Suwon 16499, South Korea*; orcid.org/0000-0002-8125-6141; Email: jsheo@ajou.ac.kr

Authors

Jungho Ahn − *Department of Electrical and Computer Engineering, Ajou University, Suwon 16499, South Korea*

Jiyeon Ma − *School of Electronic Engineering, Soongsil University, Seoul 06938, South Korea*; orcid.org/0000-0002-8997-2951

Doeon Lee − *Department of Electrical and Computer Engineering, University of Virginia, Charlottesville, Virginia 22904, United States*

Qiubao Lin − *School of Science, Jimei University, Xiamen 361021, China*

Youngseo Park − *Department of Electrical and Computer Engineering, Ajou University, Suwon 16499, South Korea*

Oukjae Lee − *Center for Spintronics, Korea Institute of Science and Technology (KIST), Seoul 02792, South Korea*

Sangwan Sim − *Division of Electrical Engineering, Hanyang University, Ansan 15588, South Korea*

Complete contact information is available at: https://pubs.acs.org/10.1021/acsphotonics.0c01579

Author Contributions

J.A., J.M., D.L., and Q.L. equally contributed to this work. J.M. and Y.P. fabricated the devices and conducted the temperature-dependent electrical characterization. D.L., Y.P., G.Y., and J.H. contributed to the analysis of the results. G.Y. and J.H. proposed the work and directed the study. All authors contributed to the writing of the manuscript.

Notes

The authors declare no competing financial interest.

ACKNOWLEDGMENTS

This study was supported by the Industrial Strategic Technology Development Program (20000300) funded by the Ministry of Trade, Industry, and Energy (MOTIE, Republic of Korea) and by the Human Resources Program in Energy Technology of the Korea Institute of Energy Technology Evaluation and Planning, which granted us financial resources from the MOTIE, Republic of Korea (20184030202220). D.L. and K.L. were supported by the U.S. National Science Foundation (NSF) under grant CMMI-1825256.

REFERENCES

(1) Hirano, A.; Pernot, C.; Iwaya, M.; Detchprohm, T.; Amano, H. Demonstration of Flame Detection in Room Light Background by Solar-Blind AlGaN PIN Photodiode. *phys. stat. sol* **2001**, *188* (1), 293−296.

(2) Liu, E.; Long, M.; Zeng, J.; Luo, W.; Wang, Y.; Pan, Y.; Zhou, W.; Wang, B.; Hu, W.; Ni, Z.; You, Y.; Zhang, X.; Qin, S.; Shi, Y.; Watanabe, K.; Taniguchi, T.; Yuan, H.; Hwang, H. Y.; Cui, Y.; Miao, F.; Xing, D. High Responsivity Phototransistors Based on Few-Layer ReS2 for Weak Signal Detection. *Adv. Funct. Mater.* **2016**, *26* (12), 1938−1944.

(3) Tsai, S.; Basu, S.; Huang, C.; Hsu, L.; Lin, Y. Deep-Ultraviolet Photodetectors Based on Epitaxial ZnGa2O4 Thin Films. *Sci. Rep.* **2018**, *8*, 14056.

(4) Teng, Y.; Song, L. X.; Liu, W.; Xu, Z. Y.; Wang, Q. S.; Ruan, M. M. Monodispersed Hierarchical ZnGaM2O4Microflowers for Self-Powered Solar-Blind Detection. *J. Mater. Chem. C* **2016**, *4*, 3113.

(5) Soltani, A.; Barkad, H. A.; Mattalah, M.; Benbakhti, B.; Jaeger, J. De; Chong, Y. M.; Zou, Y. S.; Zhang, W. J.; Lee, S. T.; Benmoussa, A.; Giordanengo, B. 193 Nm Deep-Ultraviolet Solar-Blind Cubic Boron Nitride Based Photodetectors. *Appl. Phys. Lett.* **2008**, *92*, 053501.

(6) Koide, Y.; Liao, M.; Alvarez, J. Thermally Stable Solar-Blind Diamond UV Photodetector. *Diamond Relat. Mater.* **2006**, *15*, 1962−1966.

(7) Liao, M.; Koide, Y. High-Performance Metal-Semiconductormetal Deep-Ultraviolet Photodetectors Based on Homoepitaxial Diamond Thin Film. *Appl. Phys. Lett.* **2006**, *89*, 113509.

(8) Oshima, T.; Okuno, T.; Arai, N.; Suzuki, N.; Hino, H.; Fujita, S. Related Content Flame Detection by a β-Ga2O3-Based Sensor. *Jpn. J. Appl. Phys.* **2009**, *48*, 011605.

(9) Razeghi, M.; Member, S. Short-Wavelength Solar-Blind Detectors-Status, Prospects, and Markets. *Proc. IEEE* **2002**, *90* (6), 1006−1014.

(10) Cho, C.-Y.; Zhang, Y.; Cicek, E.; Rahnema, B.; Bai, Y.; McClintock, R.; Razeghi, M. Surface Plasmon Enhanced Light Emission from AlGaN-Based Ultraviolet Light-Emitting Diodes Grown on Si (111). *Appl. Phys. Lett.* **2013**, *102*, 211110.

(11) Chen, X.; Ren, F.; Gu, S.; Ye, J. Review of Gallium-Oxide-Based Solar-Blind Ultraviolet Photodetectors. *Photonics Res.* **2019**, *7* (4), 381.

(12) Tsao, J. Y.; Chowdhury, S.; Hollis, M. A.; Jena, D.; Johnson, N. M.; Jones, K. A.; Kaplar, R. J.; Rajan, S.; Van de Walle, C. G.; Bellotti, E.; Chua, C. L.; Collazo, R.; Coltrin, M. E.; Cooper, J. A.; Evans, K. R.; Graham, S.; Grotjohn, T. A.; Heller, E. R.; Higashiwaki, M.; Islam, M. S.; Simmons, J. A. Ultrawide-Bandgap Semiconductors: Research Opportunities and Challenges. *Adv. Electron. Mater.* **2018**, *4*, 1600501.

(13) Choopun, S.; Vispute, R. D.; Yang, W.; Sharma, R. P.; Venkatesan, T.; Shen, H. Realization of Band Gap above 5.0 EV in Metastable Cubic-Phase MgxZn1-XO Alloy Films. *Appl. Phys. Lett.* **2002**, *80*, 1529−1531.

(14) Yang, W.; Hullavarad, S. S.; Nagaraj, B.; Takeuchi, I.; Sharma, R. P.; Venkatesan, T.; Vispute, R. D.; Shen, H. Compositionally-Tuned Epitaxial Cubic on Si (100) for Deep Ultraviolet Photodetectors. *Appl. Phys. Lett.* **2003**, *82*, 3424.

(15) Aida, H.; Nishiguchi, K.; Takeda, H.; Aota, N.; Sunakawa, K.; Yaguchi, Y. Related Content Growth of β-Ga2O3 Single Crystals by the Edge- Defined, Film Fed Growth Method. *Jpn. J. Appl. Phys.* **2008**, *47*, 8506.

(16) Higashiwaki, M.; Sasaki, K.; Murakami, H. Recent Progress in Ga2O3 Power Devices. *Semicond. Sci. Technol.* **2016**, *31*, 034001.

(17) Villora, E. G.; Shimamura, K.; Yoshikawa, Y.; Aoki, K.; Ichinose, N. Large-Size β-Ga_2O_3 Single Crystals and Wafers. *J. Cryst. Growth* **2004**, *270*, 420−426.

(18) Tomm, Y.; Reiche, P.; Klimm, D.; Fukuda, T. Czochralski Grown Ga_2O_3 Crystals. *J. Cryst. Growth* **2000**, *220*, 510−514.

(19) Oh, S.; Kim, C.-K.; Kim, J. High Responsivity β-Ga2O3Metal−Semiconductor−Metal Solar-Blind Photodetectors with Ultraviolet Transparent Graphene Electrodes. *ACS Photonics* **2018**, *5*, 1123−1128.

(20) Oh, S.; Mastro, M. A.; Tadjer, M. J.; Kim, J. Solar-Blind Metal-Semiconductor-Metal Photodetectors Based on an Exfoliated β-

Ga2O3Micro-Flake. *ECS J. Solid State Sci. Technol.* **2017**, *6*, Q79−Q83.
(21) Liu, Y.; Du, L.; Liang, G.; Mu, W.; Jia, Z.; Xu, M.; Xin, Q. β-Ga_2O_3 Field-Effect-Transistor-Based Solar-Blind Photodetector With Fast Response and High Photo-to-Dark Current Ratio. *IEEE Electron Device Lett.* **2018**, *39* (11), 1696−1699.
(22) Pratiyush, A. S.; Xia, Z.; Kumar, S.; Zhang, Y.; Joishi, C. MBE-Grown β-Ga2O3-Based Schottky UV-C Photodetectors With Rectification Ratio 10^7. *IEEE Photonics Technol. Lett.* **2018**, *30* (23), 2025−2028.
(23) Fang, H.; Hu, W. Photogating in Low Dimensional Photodetectors. *Adv. Sci.* **2017**, *4*, 1700323.
(24) Oshima, T.; Okuno, T.; Arai, N.; Suzuki, N.; Ohira, S.; Fujita, S. Vertical Solar-Blind Deep Ultraviolet Schottky Photodetectors Based on β-Ga2O3 Substrates. *Appl. Phys. Express* **2008**, *1*, 011202.
(25) Wei, T.; Tsai, D.; Ravadgar, P.; Ke, J.; Tsai, M.; Lien, D. See-Through β-Ga2O3 Solar-Blind Photodetectors for Use in Harsh Environments. *IEEE J. Sel. Top. Quantum Electron.* **2014**, *20* (6), 112−117.
(26) Kim, S.; Oh, S.; Kim, J. Ultrahigh Deep-UV Sensitivity in Graphene-Gated β-Ga2O3 Phototransistors. *ACS Photonics* **2019**, *6*, 1026−1032.
(27) Kong, W.; Wu, G.; Wang, K.; Zhang, T.; Zou, Y.; Wang, D.; Luo, L. Graphene-β-Ga2O3 Heterojunction for Highly Sensitive Deep UV Photodetector Application. *Adv. Mater.* **2016**, *28*, 10725−10731.
(28) Zhao, B.; Wang, F.; Chen, H.; Wang, Y.; Jiang, M.; Fang, X.; Zhao, D. Solar-Blind Avalanche Photodetector Based On Single ZnO−Ga2O3 Core−Shell Microwire. *Nano Lett.* **2015**, *15*, 3988−3993.
(29) Lee, J. H.; Eun, J. H.; Park, S. Y.; Kim, S. G.; Kim, H. J. Hydration of r.f. Magnetron Sputtered MgO Thin Films for a Protective Layer in AC Plasma Display Panel. *Thin Solid Films* **2003**, *435*, 95−101.
(30) Tigunta, S.; Sando, D.; Chanlek, N.; Supadee, L.; Pojprapai, S. Effect of Gas Atmospheres on Degradation of MgO Thin Film Magnetic Tunneling Junctions by Deionized Water. *Thin Solid Films* **2020**, *709*, 138185.
(31) Wang, X.; Shao, Y.; Wu, X.; Zhang, M.; Li, L.; Liu, W.; Zhang, D. W.; Ding, S. Light Response Behaviors of Amorphous In−Ga−Zn−O Thin-Film Transistors via in Situ Interfacial Hydrogen Doping Modulation. *RSC Adv.* **2020**, *10*, 3572−3578.
(32) Hung, M. P.; Wang, D.; Jiang, J.; Furuta, M. Negative Bias and Illumination Stress Induced Electron Trapping at Back-Channel Interface of InGaZnO Thin-Film Transistor. *ECS Solid State Lett.* **2014**, *3* (3), Q13−Q16.
(33) Ji, K. H.; Kim, J.; Mo, Y.; Jeong, J. H.; Yang, S.; Hwang, C.; Park, S. K.; Ryu, M.; Lee, S.; Jeong, J. K. Comparative Study on Light-Induced Bias Stress Instability of IGZO Transistors With SiN x and SiO 2 Gate Dielectrics. *IEEE Electron Device Lett.* **2010**, *31* (12), 1404−1406.
(34) Choi, S.-H.; Han, M.-K. Effect of Channel Widths on Negative Shift of Threshold Voltage, Including Stress-Induced Hump Phenomenon in InGaZnO Thin-Film Transistors under High-Gate and Drain Bias Stress. *Appl. Phys. Lett.* **2012**, *100*, 043503.
(35) Mativenga, M.; Seok, M.; Jang, J. Gate Bias-Stress Induced Hump-Effect in Transfer Characteristics of Amorphous-Indium-Galium-Zinc-Oxide Thin-Fim Transistors with Various Channel Widths. *Appl. Phys. Lett.* **2011**, *99*, 122107.
(36) Jeong, J. K. The Status and Perspectives of Metal Oxide Thin-Film Transistors for Active Matrix Flexible Displays. *Semicond. Sci. Technol.* **2011**, *26*, 034008.
(37) Zhou, H.; Si, M.; Alghamdi, S.; Qiu, G.; Yang, L.; Ye, P. D. High-Performance Depletion/Enhancement-Mode β-Ga2O3 on Insulator (GOOI) Field-Effect Transistors With Record Drain Currents of 600/450 MA/Mm. *IEEE Electron Device Lett.* **2017**, *38* (1), 103−106.
(38) Armstrong, A. M.; Crawford, M. H.; Jayawardena, A. Role of Self-Trapped Holes in the Photoconductive Gain of β-Gallium Oxide Schottky Diodes. *J. Appl. Phys.* **2016**, *119*, 103102.
(39) Qi, Z.; Yang, T.; Li, D. High-Responsivity Two-Dimensional p-PbI2/n-WS2 Vertical Heterostructure Photodetectors Enhanced by Photogating Effect. *Mater. Horiz.* **2019**, *6*, 1474−1480.
(40) Guo, N.; Gong, F.; Liu, J.; Jia, Y.; Zhao, S.; Liao, L.; Su, M.; Fan, Z.; Chen, X.; Lu, W.; Xiao, L.; Hu, W. Photogating_Hybrid WSe2−In2O3 Phototransistor with Ultrahigh Detectivity. *ACS Appl. Mater. Interfaces* **2017**, *9*, 34489−34496.
(41) Roul, B.; Kumar, M.; Rajpalke, M.; Bhat, T. Binary Group III-Nitride Based Heterostructures : Band Offsets and Transport Properties. *J. Phys. D: Appl. Phys.* **2015**, *48*, 423001.
(42) Smith, J.; Naruse, J.; Hidehiko, H.; Siegel, D. Intrinsic Conductivity in Magnesium−Oxygen Battery Discharge Products: MgO and MgO2. *Chem. Mater.* **2017**, *29* (7), 3152−3163.
(43) Mohamed, M.; Irmscher, K.; Janowitz, C.; Galazka, Z.; Manzke, R.; Fornari, R. Schottky Barrier Height of Au on the Transparent Semiconducting Oxide β-Ga2O3. *Appl. Phys. Lett.* **2012**, *101*, 132106.
(44) Jeon, S.; Ahn, S.; Song, I.; Kim, C. J.; Chung, U.; Lee, E.; Yoo, I.; Nathan, A.; Lee, S.; Gha, K.; Robertson, J.; Kim, K. Gated Three-Terminal Device Architecture to Eliminate Persistent Photoconductivity in Oxide Semiconductor Photosensor Arrays. *Nat. Mater.* **2012**, *11*, 301−305.
(45) Jin, C.; Kim, H.; Lee, W. I.; Lee, C. Ultraintense Luminescence in Semiconducting-Material- Sheathed MgO Nanorods. *Adv. Mater.* **2011**, *23*, 1982−1987.
(46) Yun, M. G.; Kim, Y. K.; Ahn, C. H.; Cho, S. W.; Kang, W. J. Low Voltage-Driven Oxide Phototransistors with Fast Recovery, High Signal-to-Noise Ratio, and High Responsivity Fabricated via a Simple Defect-Generating Process. *Sci. Rep.* **2016**, *6*, 31991.
(47) Shao, Z.; Jiang, T.; Zhang, X.; Zhang, X.; Lee, S.; Jie, J.; Wu, X.; Xia, F.; Xiong, S. Memory Phototransistors Based on Exponential-Association Photoelectric Conversion Law. *Nat. Commun.* **2019**, *10*, 1294.
(48) Ju, L.; Jr, J. V.; Huang, E.; Kahn, S.; Nosiglia, C.; Tsai, H.; Yang, W.; Taniguchi, T.; Watanabe, K.; Zhang, Y.; Zhang, G.; Crommie, M.; Zettl, A.; Wang, F. Photoinduced Doping in Heterostructures of Graphene and Boron Nitride. *Nat. Nanotechnol.* **2014**, *9* (5), 348−352.
(49) Li, L.; Auer, E.; Liao, M.; Fang, X.; Zhai, T.; Gautam, U. K. Deep-Ultraviolet Solar-Blind Photoconductivity of Individual Gallium Oxide Nanobelts. *Nanoscale* **2011**, *3*, 1120−1126.
(50) Pratiyush, A. S.; Krishnamoorthy, S.; Vishnu Solanke, S.; Xia, Z.; Muralidharan, R.; Rajan, S.; Nath, D. N. High Responsivity in Molecular Beam Epitaxy Grown β-Ga2O3Metal Semiconductor Metal Solar Blind Deep-UV Photodetector. *Appl. Phys. Lett.* **2017**, *110*, 221107.
(51) Nakagomi, S.; Momo, T.; Takahashi, S.; Kokubun, Y. Deep Ultraviolet Photodiodes Based on β-Ga2O3/SiC Heterojunction. *Appl. Phys. Lett.* **2013**, *103*, 072105.
(52) Feng, W.; Wang, X.; Zhang, J.; Wang, L.; Zheng, W.; Hu, P.; Caob, W.; YangbBin. Synthesis of Two-Dimensional b-Ga2O3 Nanosheets for High-Performance Solar Blind Photodetectors. *J. Mater. Chem. C* **2014**, *2*, 3254−3259.
(53) Zhao, B.; Fei, W.; Hongyu, C.; Lingxia, Z.; Longxing, S.; Zhao, D.; Fang, X. An Ultrahigh Responsivity (9.7 MA W−1) Self-Powered Solar-Blind Photodetector Based on Individual ZnO−Ga2O3 Heterostructures. *Adv. Funct. Mater.* **2017**, *27*, 1700264.
(54) Chen, X.; Mi, W.; Wu, J.; Yang, Z.; Zhang, K.; Zhao, J.; Luan, C.; Wei, Y. A Solar-Blind Photodetector Based on β-Ga2O3 Film Deposited on MgO (100) Substrates by RF Magnetron Sputtering. *Vacuum* **2020**, *180*, 109632.
(55) Wang, H.; Chen, H.; Li, L.; Wang, Y.; Su, L.; Bian, W.; Li, B.; Fang, X. High Responsivity and High Rejection Ratio of Self-Powered Solar- Blind Ultraviolet Photodetector Based on PEDOT:PSS/β-Ga2O3 Organic/Inorganic P−n Junction. *J. Phys. Chem. Lett.* **2019**, *10*, 6850−6856.

https://dx.doi.org/10.1021/acsphotonics.0c01579
ACS Photonics 2021, 8, 557−566

(56) Yu, J.; Wang, Y.; Li, H.; Huang, Y.; Tang, W. Tailoring the Solar-Blind Photoresponse Characteristics of β-Ga2O3 Epitaxial Films through Lattice Mismatch and Crystal Orientation. *J. Phys. D: Appl. Phys.* **2020**, *53*, 24LT01.
(57) Arora, K.; Goel, N.; Kumar, M.; Kumar, M. Ultrahigh Performance of Self-Powered B-Ga2O3 Thin Film Solar-Blind Photodetector Grown on Cost-Effective Si Substrate Using High Temperature Seed Layer. *ACS Photonics* **2018**, *5*, 2391−2401.

https://dx.doi.org/10.1021/acsphotonics.0c01579
ACS Photonics 2021, 8, 557−566